(NASA-CR-158792) SATELLITE PASSIVE REMOTE SENSING OF OFF-SHORE POLLUTANTS, VOLUME 2 Final Report (University of Southern California) 46 p HC A03/MF A01 CSCL 13B

N79-27634

Unclas
G3/43 29253

VOLUME II: SATELLITE PASSIVE REMOTE SENSING OF OFF-SHORE POLLUTANTS

(of 2 volumes)

Prepared for: Beverly Lewis
NASA Langley Research Center
Langley Field, Bldg. 1201
Mail Stop 404B
Langley, VA 23300

As a Final Technical Report under: Grant NSG 1528
"Remote Sensing of Ocean Pollutants"

Institute for Marine and Coastal Studies
University of Southern California
University Park
Los Angeles, CA 90007

June, 1979

TABLE OF CONTENTS

SATELLITE PASSIVE REMOTE SENSING OF OFF-SHORE POLLUTANTS

INTRODUCTION

In this report we discuss satellite detection and monitoring of off-shore dumped pollutants, other than oil. Following EPA guidelines, we divide the pollutants into four categories:

- acid waste
- industrial waste
- sewage sludge
- dredge material

Off-shore dumps consist of material that sink, or at the very least do not remain on the water surface. Of the three portions of the spectrum, visible, infrared and microwave, only the first that penetrates the water can sense waste concentration. The major problem in the visible band is to get around weather and atmospheric haze.

The results of the analyses in this report confirm the intuitive notion that all three satellite based sensors have the required sensitivity to do the job, but only the visible has sufficient spatial resolution. However, none of the sensing techniques allow a clean cut extraction of the pollutant signature from the background. We assert that the problem of pollution monitoring is <u>not</u> a sensor problem but a <u>problem of mathematical modeling and data processing</u>.

Part 1 of this report presents summaries of satellite sensor performance in three spectral bands, visible, infrared, and microwave. Part 2, the bulk of the report gives all the calculations, trade-offs and limitations of the three sensor systems.

PART 1: SUMMARY OF SATELLITE PASSIVE SENSORS

SATELLITE PASSIVE SENSORS

	Visible	Infrared	Microwave
Wavelength	510 nm 680 nm	10.6μm 3.8μm	1 cm (30 GHz)
Spectral Band	30 nm	2μm .8μm	3 GHz
Sensor Number or Area	100 cm^2	100 sensors	N sensors
Dwell Time	38s	150μs	150 N μsec
Collecting Aperture	10 cm diameter	30 cm diameter	10 m diameter
Sensitivity	Min. Det. Cont. = .04%	10 mk 50 mk	.5K
Efficiency	1%	50%	-----
Spatial Resolution	30 m x 30 m	100m x 100m 240m x 240m	1 km x 1 km
Altitude	1 Mm	1 Mm	1 Mm
Swath Width crosstrack	1 Mm	1 Mm	1 Mm
downtrack	10 km	NA	NA

PART 2: SENSORS TRADE-OFF

In the following we present the results of our trade-off between sensitivity and resolution for three satellite based sensors

- visible imaging radiometer
- infrared scanning radiometer
- microwave scanning radiometer

1.0 OPTICAL RADIOMETRY

We have studied satellite sensors to investigate the feasibility of seeing low-contrast patterns in color on the sea surface. The feasibility divides into two questions. First, what existing or planned sattelites provide a capability suitable for a demonstration. The short answer is that NASA LandSat D scheduled for launch in 1983 should provide 3% contrast in a 30 x 30 meter pixel, slightly smeared in the crosstrack direction by limited electronic response time.

The second question is, What capability can be achieved in a satellite package optimized for pollution detection? In this case NASA's present radiometric methods are inappropriate because they have traded off contrast and resolution in order to achieve absolute radiometric calibration. If we forego absolute measurements, it is possible to optimize for recognition of low-contrast patterns that represent spilled pollutant. This leads to a sensor that performs more like a low-light-level television system.

The following sections address the two questions. The first describes the radiometer aboard LandSat D, and the second describes possibilities for a system dedicated to the pollution detection problem.

1.1 LandSat D: Thematic Mapper

This satellite carries a radiometer that scans a swath 100 nautical miles wide on the earth's surface. In the visible range of interest are two color bands, a blue-green one from 450 to 520 nm and yellow-orange from 520 to 600 nm. Each band uses an array of 16 silicon photodiodes as detectors. A mechanical scanner sweeps the crosstrack direction while orbital motion scans along track.

The relevant properties of the LandSat D radiometer appear in Table 1 along with the symbols used to denote these quantities in the equations

TABLE 1: PROPERTIES OF LandSat D

Swath width: S = 185 km

Altitude: H = 1 Mm

Velocity, equivalent surface: V = 6.6 km/sec

Detectors in array: N = 16

Footprint (square pixel) size: δ = 30 meters

Dwell time: τ = 10μsec

Spectral radiance of the sea: L_λ = 0.035 W/sr/m^2/nm

Filter pass, Band 1: b = 80 nm

Telescope efficiency: η = 0.2

Aperture diameter: d = 40 cm

Detector responsivity: R = 0.6/volt

Thermal noise, spectral density: kT = 4 x 10^{-21} watt/Hz

(T = 290 kelvin)

Electron's charge: e = 1.6 x 10^{-19} coulomb

Detector/amplifier bandwidth: B = 50 kHz

Noise resistance: R = 1.0 x 10^9 ohms

(feedback resistor for transimpedance amplifier)

that follow. The area coverage rate is the product of velocity V by swath width S:

$$\dot{A} = VS = 1220 \text{ km}^2/\text{sec},$$

From this we derive the dwell time τ that one of the 16 sensors inspects each pixel (δ by δ) on the sea surface:

$$\tau = N\delta^2/\dot{A} = 10\mu\text{sec}$$

Note that $N\delta^2$ is the footprint of the N sensors on the earth surface.

The scene (sea and air above it) has a certain radiance L (watt/m^2/steradian) that is focused on the detector where power p produces current I:

$$p = L \text{ (efficiency) (area) (solid angle)}$$

$$\text{(solid angle)} = \text{(aperture area/altitude}^2\text{)} = \pi d^2/4H^2$$

$$p = L\eta\delta^2 \, (\pi d^2/4H^2)$$

$$\frac{p}{L} = \frac{\pi}{4} \eta \left(\frac{\delta d}{h}\right)^2 = 22.6 \times 10^{-12} \text{ m}^2 \qquad (1)$$

The light detector is a silicon photodiode that converts electric current with typical responsivity R = 0.6 amps/watt. To facilitate calculations that follow, we use one factor K to convert sea radiance to detector current I:

$$K \equiv \frac{I}{L} = \frac{I}{p} \frac{p}{L} = R \frac{p}{L} = 13.6 \times 10^{-12} \text{ m}^2\text{sr/volt} \qquad (2)$$

We shall estimate the noise current i_n in the detector and use K to convert it to a minimum detectable radiance (MDL) on the sea surface:

$$MDL = i_n/K \qquad (3)$$

Two types of noise limit performance of the system, shot and thermal (Johnson), given by the following:

$$i_s^2 = 2eIB \tag{4a}$$

$$i_t^2 = 4kTB/R \tag{4b}$$

$$i_n^2 = i_s^2 + i_t^2 \tag{5}$$

Here R is the load resistance across the photodiode, or the feedback resistance in the case of a circuit with a transimpedance amplifier. Normally thermal noise would limit the performance of a photodiode, but in this case NASA has used a newly developed sensor with a transimpedance amplifier. The equivalent noise resistance is remarkably high, $R = 10^9$ ohms.

Substituting Eqs. 4a and 4b in 5, and using Eqs. 2 and 3 gives

$$MDL = \sqrt{(C_1 + C_2 L)\, B} \tag{6}$$

where

$$C_1 = 4kT/K^2R \qquad C_2 = 2e/K \tag{7}$$

and

$$C_1 B = 4.35 \times 10^{-3}\ (W/m^2/sr)^2$$

$$C_2 B = 1.18 \times 10^{-3}\ W/m^2/sr \tag{8}$$

We have plotted Eq. 6 in Figure 1 in the form MDL/L, which is the minimum detectable contrast. One point on this curve is particularly significant at a radiance of $L_s = 2.8\ W/m^2/sr$. This value is typical of scene radiance looking at open ocean (no clouds). The minimum detectable

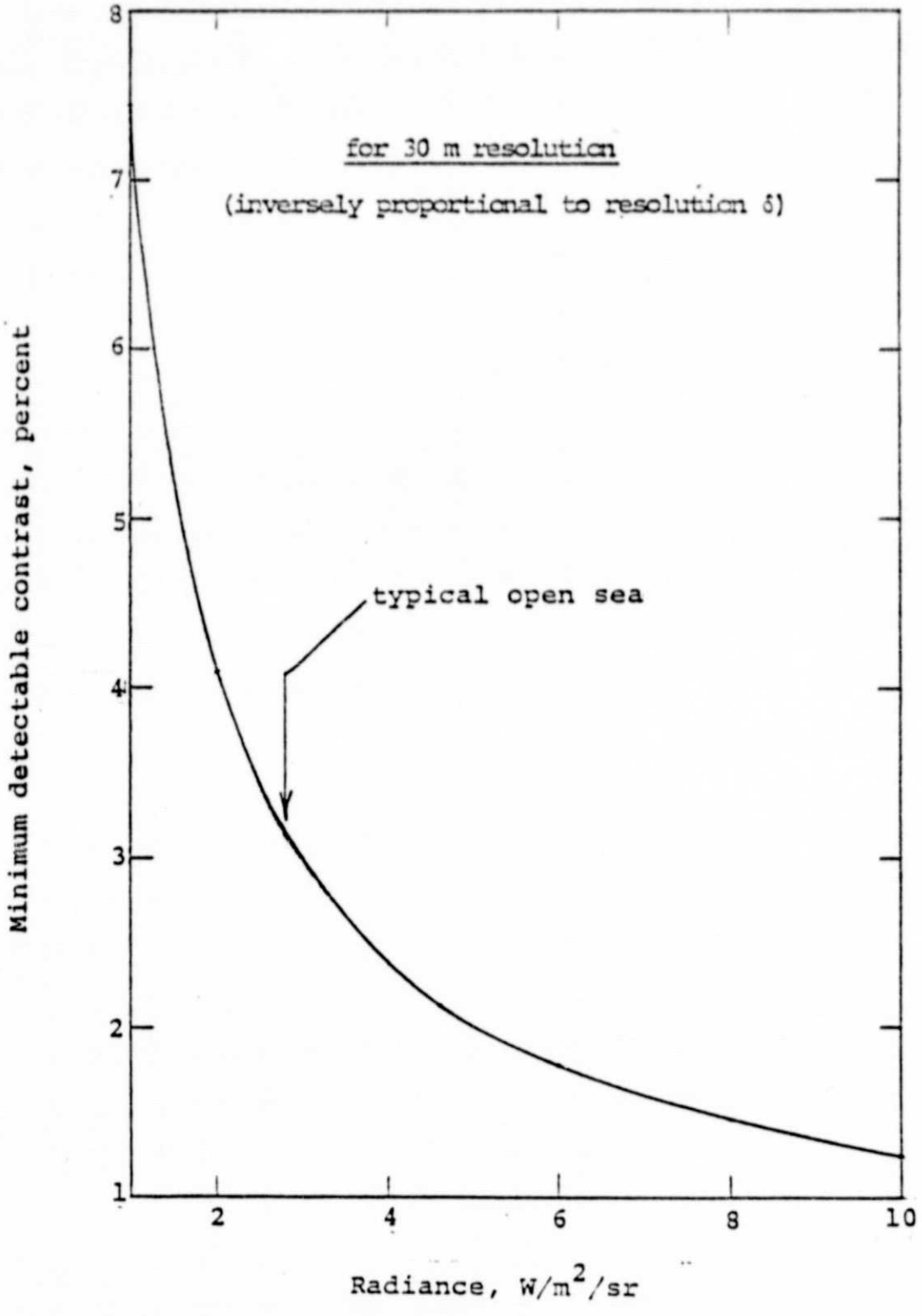

Fig. 1. Minimum detectable contrast in thematic mapper, LandSat D

contrast is 3.1%, and its reciprocal is the signal-to-noise ratio in terms of photocurrent (I/i_n), namely 32. It happens that NASA has specified this same signal-to-noise ratio at the same radiance in its contract with Hughes Santa Barbara Research Center. The saturation radiance is 10 $W/m^2/sr$ at which the specified signal-to-noise is 85, a bit higher than our estimate of 79 (reciprocal of 1.3% in Figure 1).

We estimated the radiance of the sea by first averaging its spectral radiance (see in Figures 12, 13 and 14 of Roswell Austin's paper in Optical Aspects of Oceanography, edited by Jerlov and Nielsen and reproduced in the Appendix). The average spectral radiance L_λ = 0.035 $W/m^2/sr/nm$, multiplied by the filter pass band, b = 80 nm, then gives the result we used:

$$L_s = L_\lambda b = 2.8\ W/m^2/sr. \quad \text{(in the blue-green)}$$

The same graphs indicate that only 14% (a seventh) of the light comes from the sea surface; the rest is backscattered by air. Of the part from the sea, about a third is surface reflection. Thus 10% of the radiance at the radiometer is light that has penetrated the sea. Presumably this percentage is improved by avoiding sun glint.

Finally, the frequency response of the thematic mapper rolls off at B = 50kHz = $1/2\tau$, and so the radiance in one pixel spills over a bit into the next one or two pixels in the crosstrack scan direction.

1.2 Dedicated Imaging Sensor

This section discusses a satellite package dedicated to those applications in which the main problem is to see low-contrast patterns. The best approach is to use a large array of sensors to increase the dwell time on each pixel (compared to LandSat D). An ordinary television camera has in effect an array of about 250,000 sensors occupying a total area of about one square inch. It would be reasonable to assume a total photosensitive area as large as 100 cm^2, which can be divided into vari-

ous numbers of pixels (TV lines) depending on the trade-off between contrast and resolution. If common television camera tubes were used, 17 of them would be required to achieve this area in each color band i.e. 51 for a tri-color system. However, oversized tubes or some other advanced solid-state image sensor would reduce the total number of devices. We shall leave the question of size open and denote the photosensitive area by a.

A wide swath is very desirable to catch as many breaks in the clouds as possible. We assume that the width equals the altitude, i.e.

$$X = H = 1 \text{ Mm} \tag{9}$$

as shown in Figure 2. In the direction along track, the field of view is smaller to avoid excessive photosensitive area,

$$a = xy \tag{10}$$

(see Figure 2). If Y denotes the dimension of the field of view along track, then the dwell time is

$$T = Y/V \tag{11}$$

It will be advantageous to make this time as long as possible, even 10 seconds or more, to average out clutter from the sea surface. This feature requires some form of motion compensation, but the result is rewarding because it will very thoroughly remove statistical fluctuations in sun glint, and to some extent those due to patches of foam. Depending on sea state and wind, this can be a great advantage over previous NASA radiometers that essentially "freeze" the instantaneous clutter in each pixel.

Let us assume a fairly advanced system with fast optics, say a focal ratio of two:

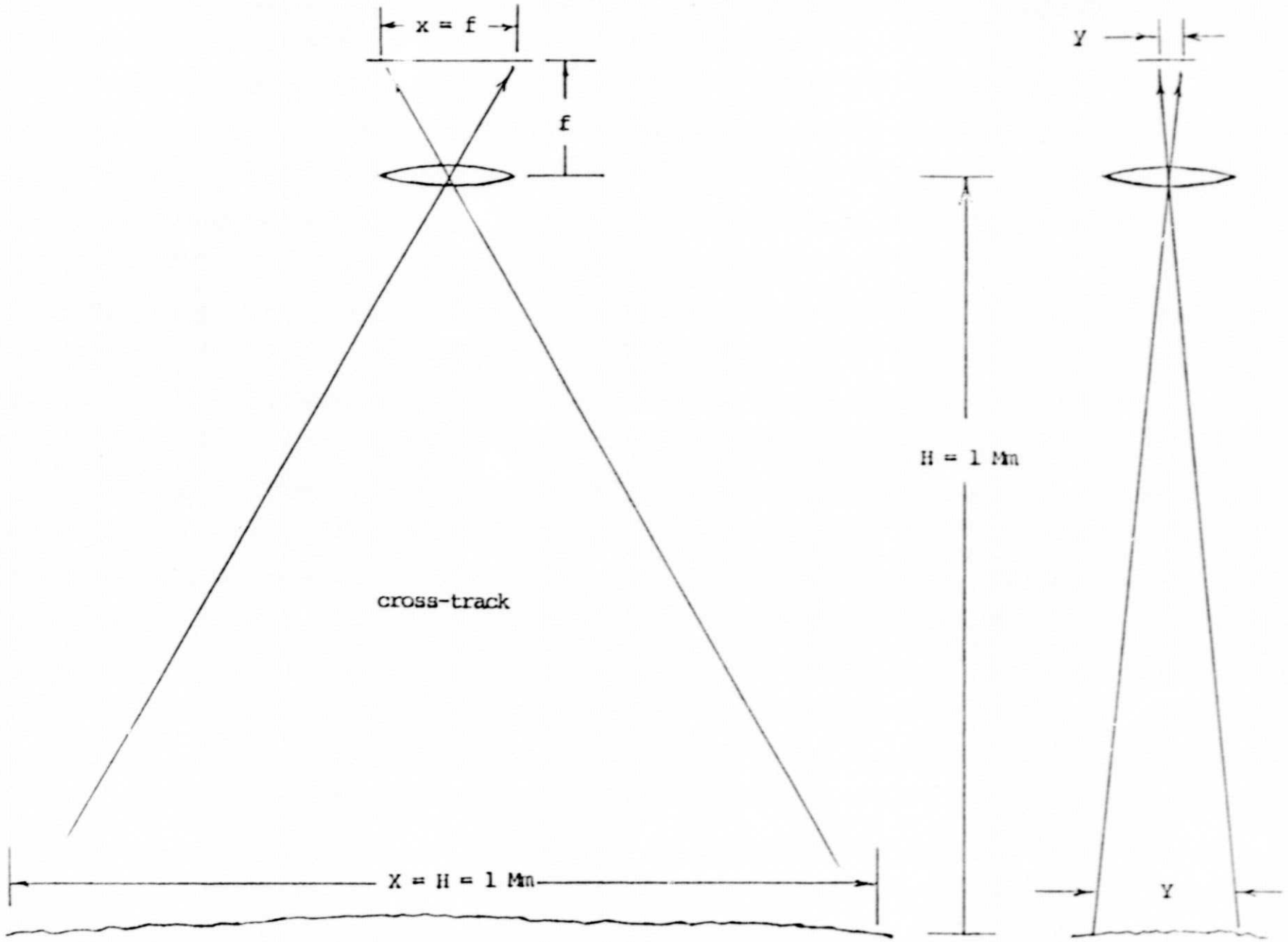

Fig. 2. Optical geometry

$$f/d = 2. \tag{12}$$

Any faster optics would not work well with an interference filter to limit the band to $\Delta\lambda = b$. Equation 12 determines the solid angle of rays into one point on the focal plane:

$$\Omega = (\pi/4)\,(d/f)^2 = \pi/16 \tag{13}$$

Apart from an optical efficiency factor η_o, the image has the same radiance as the object, namely

$$L_s = L_\lambda b \tag{14}$$

where L_λ is the spectral radiance and b the filter bandwidth. Thus the number of photons collected in the entire field of view is

$$N_\phi = (L_s/h\nu)\eta_o a\Omega\, T \tag{15}$$

and the number in each pixel is

$$n_\phi = \frac{N_\phi \delta^2}{XY} = \frac{\pi}{16}\ \frac{\eta_o L_s}{h\nu}\ \frac{a\delta^2}{VH} \tag{16}$$

where Equations 9, 11, 13 and 15 have been used.

The mean number of detection events in each pixel of the photosensitive surface is

$$n_d = n_q n_\phi \quad , \tag{17}$$

where n_q is quantum efficiency, and the standard deviation in this number is

$$\Delta n_d = \sqrt{n_d} \tag{18}$$

These equations combine to give the minimum detectable contrast

$$MDC = \frac{\Delta n_d}{n_d} = \frac{1}{\sqrt{n_q n_\phi}} \tag{19}$$

Substituting Eq. 14 in 16 in 19 gives

$$MDC = \sqrt{\frac{16}{\pi} \frac{h\nu}{\eta_o \eta_q} \frac{VH}{bL_\lambda}} \frac{1}{\delta\sqrt{a}} \tag{20}$$

Curiously, the collecting aperture d has dropped out of this expression because it is tied to f through the focal ratio, Eq. 12, and to other factors through the geometry of Figure 2.

For plotting this expression, it is convenient to put

$$L_\lambda = \ell \Lambda \tag{21}$$

where Λ is the peak spectral radiance when the sky is clear and the sun is high,

$$\Lambda = .035 \text{ W/m}^2\text{/sr/nm},$$

and ℓ represents all environmental losses of illumination due to sun angle, hydrometeors, or whatever. Finally we lump all losses of light together, whether in the environment or the equipment and put

$$\eta = \ell \eta_o \eta_d \quad . \tag{22}$$

For example, we might have

optical transparency - .5 (mostly in the filter)
20% aperture observation - .8
detector quantum efficiency - .15

sun angle - .5

haze and Rayleigh scattering - .33

---

product: $\eta = .01$

In this form, Eq. (2) becomes

$$MDC = \sqrt{\frac{16}{\pi} \frac{(h\nu)\ VH}{\eta A b}} \frac{1}{\delta\sqrt{a}} \tag{23}$$

Figure 3 shows MDC versus $\delta\sqrt{a}$ (δ in meters and $\sqrt{a}$ in cm) with η as a parameter.

For example, when

$a = 100\ cm^2$ (10 by 10 detector surface),

$\delta = 30\ m, \quad \eta = 1\%$

then $MDC = 3.8 \times 10^{-4}$.

Quite clearly this is less than the natural contrast noise on the sea due to patches of foam, seaweed, windrows, and the like. Therefore, we desire a long dwell time on each resolution cell to average out these factors as much as possible. Equation 11 gives

$$T = Y/V = (y/f)\ (H/V) \tag{24}$$

where we have used

$$Y/H = y/f \tag{25}$$

which results from similar triangles in Figure 2. The factor y/f in Eq. 24 cannot in practice be made arbitrarily large to attain a long dwell time because the motion compensation becomes nonlinear and complicated as the angles involved grow large. It is beyond the scope of this study to solve such details, but for the sake of illustration, suppose

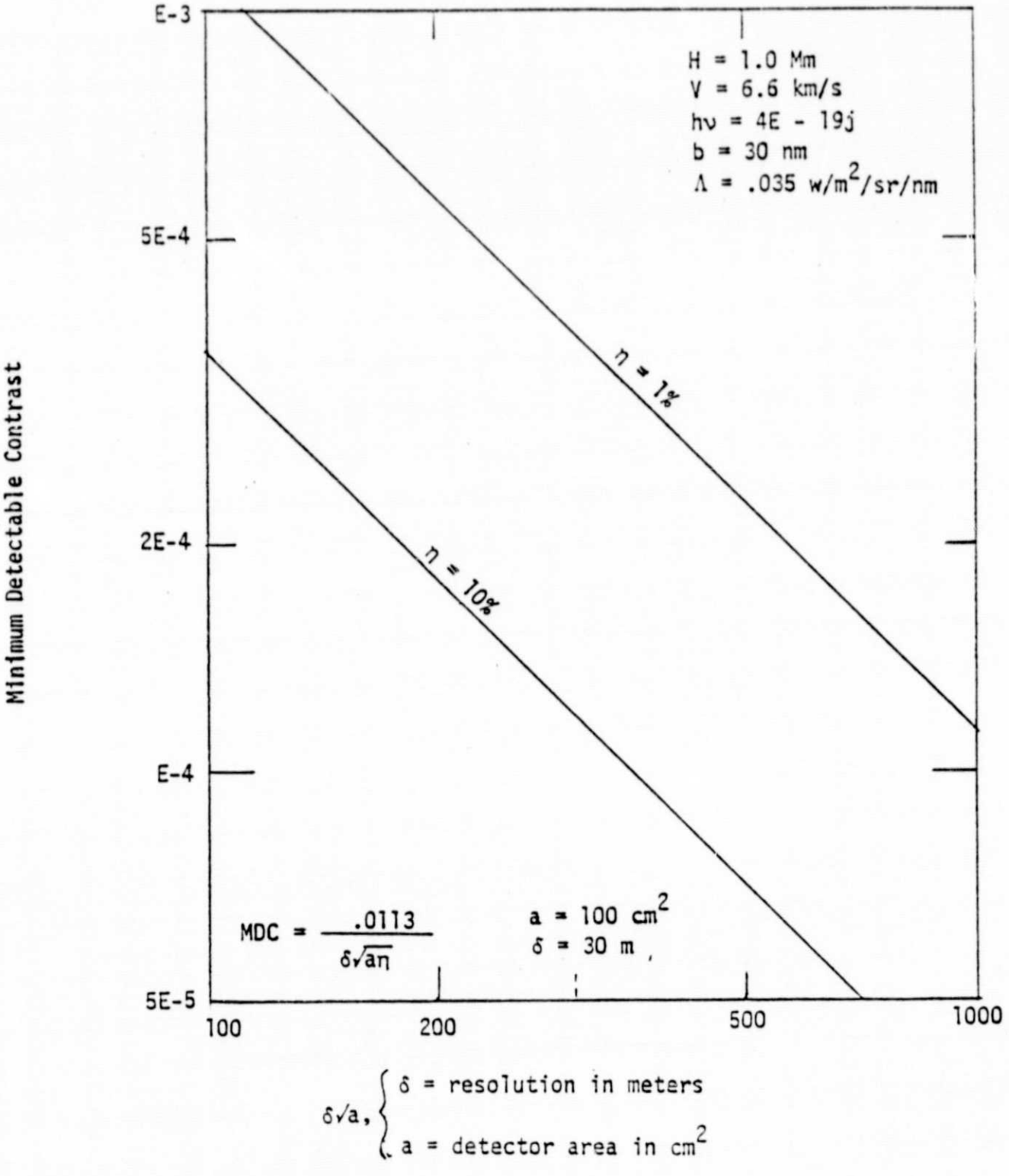

Figure 3. Minimum Detectable Contrast of Visible Radiometer

$$y/f = 1/4, \tag{26}$$

which keeps the angles quite small ($< 7^{o} = \arctan y/2f$). Then Eq. 24 gives T = 38 sec, a nice long period that averages out nearly all foam statistics as well as sun glint. Moreover, using x = f (Figure 2) and xy = a (Eq. 10), we find that

$$f = 2\sqrt{a}$$

if $a = 100\ cm^2$ (previous example) then

$$f = x = 20\ cm$$
$$y = a/x = 5\ cm$$
$$d = f/2 = 10\ cm,$$

all very small and reasonable.

For the case of an aircraft platform, we have not plotted the MDC as in Figure 3 because it is so small that it is meaningless, i.e. the product VH in Eqs. 20 and 23 is even smaller. However, the dwell time for averaging out clutter is not as long. Assuming

$$H = 3\ km\ (9840\ ft)$$
$$V = 160\ m/s$$

Equations 26 and 24 give T = 5 sec, long enough to average out sun glint, but not much else.

2.0 INFRARED SCANNING RADIOMETRY

For our purposes, "infrared" means wavelengths from 3 to 20μm. Radiation from sea and clouds in this band consists almost entirely of thermal emission, reflected and scattered sunlight being negligible. The so-called "photographic" infrared, wavelengths near 1μm, should be classed with visible light for our purposes, because this band is a component of sunlight, and so radiometry works only during the day. Within the band of interest, there are two particularly clear "windows", one at 10.6μm and the other at 3.8μm, as shown in Figure 4. The 10.6μm band (9.6 to 11.6) is the better for three reasons. First, it provides 200 times as many photons, which overpower noise in the sensor and provide more sensitivity. Second, the long wavelength has minimum sensitivity to small particles, haze and such, because Rayleigh scattering decreases as λ^4. Finally, this window has the least atmospheric absorption (from gasses and vapors) of any optical band (including visible and ultraviolet).

When the radiometer looks vertically down at the sea, it provides an almost pure measure of the temperature of the sea surface uncorrupted by other factors. Reflected sky radiance comprises only 1 or 2% of the signal at incidence angle of 0 to 30°, but this increases to 100% at grazing incidence; see Figure 5. The observed radiance originates very close to the surface, the mean distances being

$$\begin{aligned} \zeta(3.8) &= 60\mu m = 16\lambda \\ \zeta(10.6) &= 11\mu m = 1\lambda \end{aligned} \qquad (27)$$

This means that the radiometer is very sensitive to any floating pollutant, such as an oil spill that inhibits evaporation at the surface. At the very least, a coating changes the temperature by 0.5K, which is the temperature change through the so-called conduction layer, approximately the top 1.5 mm of the sea. This is a relatively large signal, but of course it is diluted with the signal from normal water wherever the film is thin and breaking up.

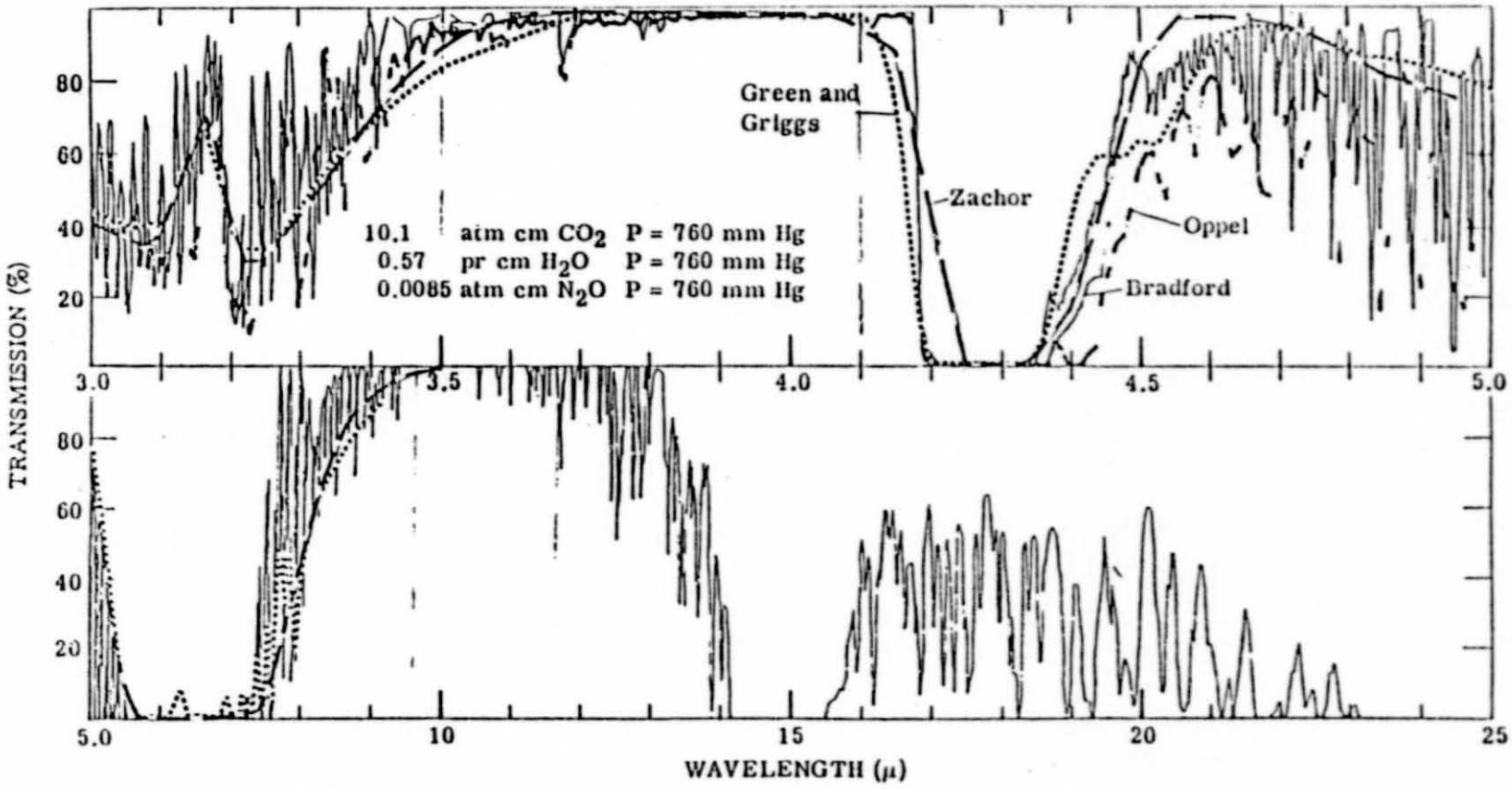

Fig. 4. Transmission over 1,000 ft Path at Sea Level

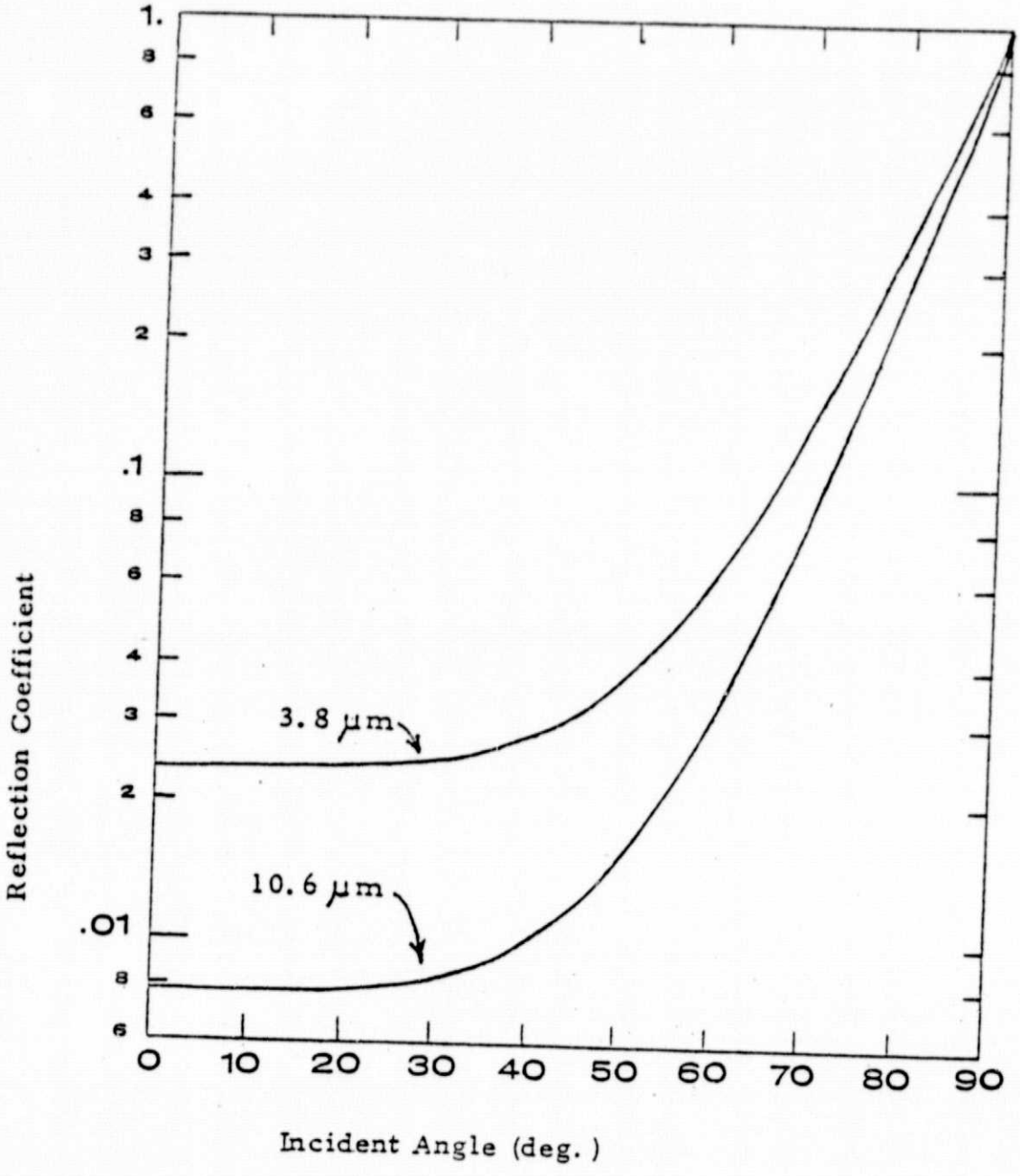

Fig. 5. Reflection Coefficient of Water

A sensitivity goal of one fiftieth this amount, i.e. 10 mK is probably appropriate. We show that an advanced satellite radiometer at 10.6μm can see a $(100\ m)^2$ resolution cell with this temperature sensitivity providing it has 100 detectors in array. A radiometer at 3.8μm would only resolve about $(240\ m)^2$. An airborne radiometer of the same design would be overkill, i.e. orders of magnitude excessive performance capability.

We doubt if the infrared radiometer has much sensitivity to pollutants that mix into bulk water, for then the surface effect is very small. There may be exceptions when the sun is shining on the water and the pollutant discolors it enough to raise the temperature by absorbing sunlight. Also, most chemicals release or absorb heat upon dilution, but this heat is a transient occurrence observable only when the dump is quite fresh.

2.1 Blackbody Formulas

The sea is very nearly a blackbody in the infrared with emissivity

$$\varepsilon_o = 1 - R_o = .98 \text{ to } .99$$

at normal incidence as discussed in connection with Figure 5. Thus it is appropriate to express radiance in terms of the blackbody function B:

$$L(\lambda) = \varepsilon B(\lambda,T) \text{ power/area/steradian}$$

However, for reasons discussed in Section 2.3, it is more appropriate to express blackbody radiation in terms of photons instead of the traditional formulas for power. We denote this change by using the symbol Q instead of B:

$$\varepsilon B \rightarrow \varepsilon Q, \text{ photons/sec/area/steradian}$$

We also denote spectral radiance with a subscript λ:

$$Q_\lambda = Q/b, \text{ ph/sec/area/sr/}\mu\text{m} \qquad (28)$$

where b is the spectral bandwidth in micrometers.

In these terms, the Planck radiation formula is

$$Q_\lambda = \frac{C_q}{\lambda 4} \exp\left(-\frac{C_e}{\lambda T}\right) \tag{29}$$

where

$$C_q \equiv 2c - 6.0E26 \text{ photons} \cdot \mu m^3/sec/m^2/sr$$
$$C_e \equiv hc/k = 14388 \mu m \cdot \text{kelvin} \tag{30}$$

Quantities useful for evaluating Equations 28, 29, and 30 in the two bands of interest appear in Table 2 above the dashed line. Those quantities involving temperature are evaluated at 295 kelvin. The choice of bandwidth b (fifth in the list) is governed by the need to avoid absorption lines in the air spectrum, Figure 4.

In all infrared radiometers, it is traditional to express the observed radiance in temperature units, i.e. the temperature of a blackbody that would give the same radiance as the observed value. This is quite natural because radiometers are calibrated by looking at a blackbody at a known temperature. Thus we need a formula to express a radiance increment ΔQ in terms of the equivalent temperature increment:

$$\Delta T = \Delta Q / Q' \tag{31}$$

where $Q' \equiv \partial Q / \partial T$. Differentiating Equation 29 gives the required expression:

$$\frac{Q'}{Q} = \frac{\partial}{\partial T} \ln Q_\lambda = \frac{C_e}{\lambda T^2} \tag{32}$$

or with the aid of Equation 31.

TABLE 2 USEFUL RADIOMETRIC QUANTITIES

evaluated at two wavelengths and T = 295 Kelvin

Quantity	Units	3.8μm	10.6μm
$C_e/\lambda = h\nu/k$	kelvin	3786	1357
$C_e/\lambda T = h\nu/kT$	(dimensionless)	12.83	4.601
$C_q/\lambda^4 = 2c/\lambda^4$	photons/s/m^2/sr/μm	2.88E24	4.75E22
Q_λ (Eq. 29)	ph/sec/m^2/sr/μm	7.67E18	4.77E20
b (suitable in air)	μm	0.6	2.0
$Q(295,\lambda) = Q_\lambda b$	ph/sec/m^2/sr	4.6E18	9.5E20
$Q/Q' = kT^2/h\nu$	kelvin	23.0	64.1
R_o (nomal incidence)	%	2.40	0.83
R_oQ/Q'	millikelvin	552	532

note only 4% difference

$$\Delta T = \frac{\Delta Q}{Q}\left(\frac{Q}{Q'}\right) = \frac{\Delta Q}{Q}\left(\frac{\lambda T^2}{C_e}\right) \tag{33}$$

or

$$\frac{\Delta T}{T} = \frac{\Delta Q}{Q}\left(\frac{\lambda T}{C_e}\right) = \frac{\Delta Q}{Q}\left(\frac{kT}{h\nu}\right) \tag{34}$$

The ratio Q/Q' for Equation 33 is listed below the dashed line in Table 2.

2.2 Natural Background Fluctuations

The last item in Table 2 gives a particularly interesting special case, the maximum effect that sky can have on the apparent temperature of the sea. Suppose the sky is completely overcast, and a radiometer beneath the overcast looks directly down at the sea. (or else a satellite radiometer looks through a small hole in the overcast) Also suppose that the temperature of the overcast is not too different from that of the sea. (A small difference, say 5K, does not matter much since the sky contributes only 1 or 2% of the radiance.) Then the sea and sky in effect form an isothermal enclosure, and the radiometer necessarily sees the thermodynamic temperature of both:

$$Q_{cloudy} = Q(T)$$

But when the sky is clear

$$Q_{clear} = \varepsilon Q(T) = (1 - R_o)\, Q(T)$$

$$\Delta Q = Q_{cloudy} - Q_{clear} = R_o Q(T)$$

and finally, using Equation 31,

$$\Delta T = \frac{\Delta Q}{Q'} = R_o \frac{Q}{Q'} \approx 540 \text{ mK} \tag{35}$$

as listed in Table 2. If the sky is partly cloudy, then the temperature increment is

$$\Delta T(f) = f(R_o Q/Q') \tag{36}$$

where f is the fraction of cloud cover. It is not easy to determine f accurately. Since the radiometer sees a blurred image of the sky in the wind-roughened sea, one cannot say exactly how much of the sky it is seeing nor to what degree. If an estimate of f is in error 10%, then the corresponding error in temperature is

$$\Delta T = 0.1\ R_o Q/Q' = 50\ mK, \tag{37}$$

which is about the maximum natural noise level for broken clouds, unless an auxillary sky radiometer is used to make a correction.

If radiometric temperature is measured at both 3.8 and 10.6μm, then there are two Equations 36 which in principle be solved for two unknowns, water temperature and fractional cloud cover. But a curious coincidence occurs as shown in Figure 6. The x and y axes represent the two unknowns, and the locus of possible values is plotted for each radiometric measurement. The intersection that fixes f and T_{sea} has such an extremely small angle that the solution is worthless in the presence of expected noise.

If the two radiometric temperatures, T(3.8) and T(10.6), are substracted, then both of the principal effects, i.e. T_{sea} and T_{sky}, are eliminated and some other residual effect remains. We do not know what the principal contribution is, but it is not roughness, as our computer simulations have shown. It may turn out that the residual is very sensitive to pollution. Perhaps it is the temperature difference resulting from different skin depths in the two bands, Equation 27. The thermal gradient from evaporation and heat conduction at the sea surface is $T = \partial T/\partial z = .33$ K/m, which gives

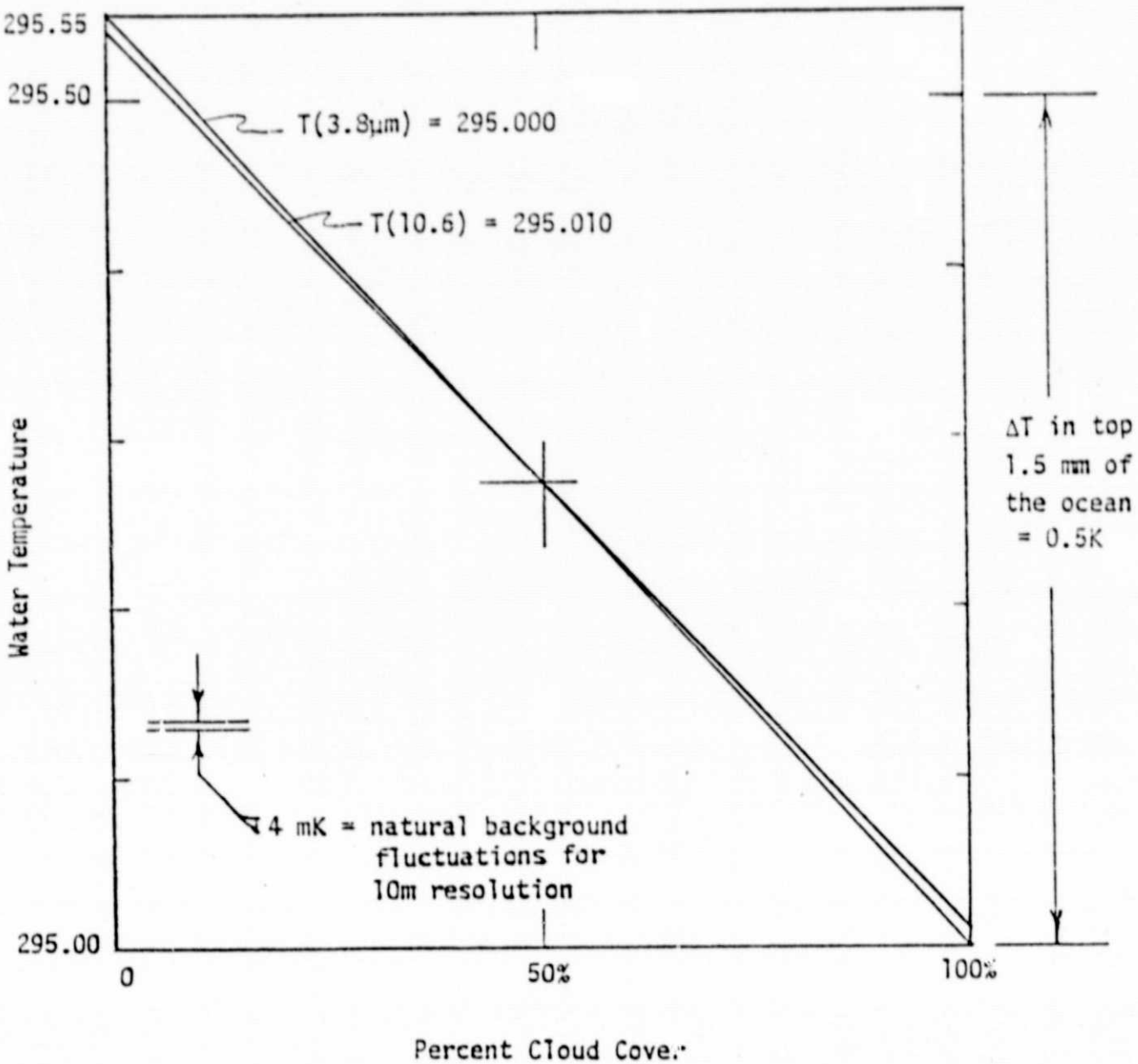

Fig. 6. Attempt to Find Both Cloud Cover and Water Temperature using Radiometric Temperature at Two Wavelengths

$$\left.\begin{aligned} \Delta_g T(3.8) &= 20 \text{ mK} \\ \Delta_g T(10.6) &= 4 \text{ mK} \end{aligned}\right\} \tag{38}$$

If the sea is not too calm, say sea state 2 or greater, then the fluctuations due to clouds, $\Delta T = 50$ mK, Equation 37 occur over large distances, comparable to the altitude of the cloud because the cloud image in the sea is blurred over about a radian. This may not interfere with the observation of pollution plumes on a smaller scale, say a few hundred meters. Over these distances the natural background noise has a variance spectrum given very roughly by

$$\left.\begin{aligned} \Phi(3\text{E-}3 \text{ cycles/m}) &= 8\text{E-}3 \text{ K}^2\text{m}^2 \\ \Phi(0.3 \text{ cycles/meter}) &= 2.3\text{E-}3 \text{ K}^2\text{m}^2 \end{aligned}\right\} \tag{39}$$

(linear interpolation (extrapolation) may be used for other frequencies). These values are very rough because they were derived from a 1-dimensional cut through space time (a ship moving at a fixed speed) in a constant field of view, and so we could only assume that the fluctuations were frozen in the sea surface as the ship moved through. In a spacial bandwidth, $\Delta\nu_x$ by $\Delta\nu_y$, the temperature variance is

$$\Delta T^2 = \Phi \Delta\nu_x \, \Delta\nu_y \tag{40}$$

If we want the temperature variance in a $(10 \text{ meter})^2$ resolution cell, it is reasonable to take

$$\Delta\nu_x = \Delta\nu_y = \frac{1/2 \text{ cycle}}{10 \text{ meters}} = .05 \text{ cycles/meter} \tag{41}$$

Then Equation 40 gives

$$\Delta T = \sqrt{6\text{E-}3 \text{ K}^2\text{m}^2} \times .05 \text{ m}^{-1} = 4 \text{ mK} \tag{42}$$

a much reduced natural background.

2.3 Radiometer Sensitivity

A satellite radiometer must be quite sophisticated compared to an aircraft radiometer. The satellite sensor collects relatively few photons from each resolution cell on the sea surface because of its high altitude and short dwell time. We assume that the satellite radiometer employs low-noise amplifiers of the type used in LandSat D and discussed in Section 1.1. In this case, the sensitivity is limited by shot noise (photon statistics) which overpowers other sources of noise, mainly thermal noise in the amplifier. (Considerably more photons are received in the infrared than a similar radiometer for visible light.) We assume that the infrared radiometer employs cold stops and a cold filter so that radiation from warm parts within the radiometer cannot reach the detector. Thus the only shot noise is that from the field of view.

The performance of infrared detectors and radiometers has traditionally been expressed in power units using figures of merit such as NEP, D and D^*. However, since the shot noise limit is both feasible and required, it is appropriate to bypass these quantities completely and discuss sensitivity in terms of photon statistics alone. It is for this reason that the preceding formulas were expressed in terms of photon flux instead of power commencing with Equation 28.

A straightforward range equation gives the number of photons collected from each resolution cell on the sea surface:

$$n_\phi = Q(\lambda) \left(\frac{\text{dwell}}{\text{time}}\right) \left(\frac{\text{cell}}{\text{area}}\right) \left(\frac{\text{solid angle subtended}}{\text{by radiometer aperture}}\right)$$

$$n = Q(\tau) (\delta^2) \left(\frac{\pi d^2/4}{H^2}\right) \tag{43}$$

where d is aperture diameter and H the radiometer's altitude. The number of detection events per all is given by

$$n_e = \eta n_\phi \tag{44}$$

where η is an overall efficiency that includes optical transparency, aperture obscuration, and detector efficiency, the last being the efficiency in converting photons to charge carriers.

Dwell time τ depends on N_d, the number of detectors in array; the more there are, the more time each detector can spend on one cell. Assuming an efficient scan pattern, i.e. each detector is always looking at a cell within the swath of interest, the dwell time is

$$\tau = \frac{\text{area examined at any instant}}{\text{area scan rate}}$$

$$\tau = \frac{N_d \delta^2}{SV} \tag{45}$$

where S denotes swath width and V the platform velocity. Substituting Equation 45 into 43 into 44 gives

$$n_e = \frac{\pi}{4} \frac{\eta N_d Q}{SV} \left(\frac{d\delta^2}{H}\right)^2 \tag{46}$$

Note the extreme sensitivity to resolution δ. This is because δ^2 enters into both the emission area and the dwell time.

Receiver sensitivity derives from the well known formula for the variance of photon (Poisson) statistics:

$$(\Delta n_e)^2 = n_e \tag{47}$$

Converting to radiometric temperature uncertainty ΔT gives

$$\frac{\Delta n_e}{n_e} = \frac{1}{\sqrt{n_e}} = \frac{\Delta Q}{Q} = \frac{\Delta T}{T} \left(\frac{C_e}{\lambda T}\right) \tag{48}$$

where Equation 47 was used in the first step, 46 in the second, and Equation 33 in the last step. Solving for ΔT gives

$$\frac{\Delta T}{T} = \frac{\lambda T}{C_e} \frac{1}{\sqrt{n_e}} \quad , \tag{49}$$

$$\frac{\Delta T}{T} = \frac{\lambda T}{C_e} \frac{4}{\pi} \sqrt{\frac{SV}{\eta N_d Q}} \frac{H}{d\delta^2} \tag{50}$$

We have plotted this equation in Figure 31 in the form ΔT versus δ with N_d as a parameter. Even though ΔT is not very sensitive to N_d, we chose it as a variable because the number of detectors varies so greatly in different arrays, all the way from 1 to 200 in a recent NASA development. Reasonable values assumed for other quantities are the following:

$T = 295$ kelvin

$C_e/\lambda T$, Q - See Table 2

$S = H = 1$ Mm

$V = 6.6$ km/sec

$\eta = 0.5$

$d = 30$ cm

Figure 7 shows that a 100-element array at 10.6μm (solid line) provides 100-meter resolution and 10 mK sensitivity. At 3.8μm (dashed lines) the performance is marginal, and either sensitivity, resolution, or both have to be compromised. On the left side of the graph the dashed lines are discontinued where the assumption of shot-noise-limited performance begins to fail.

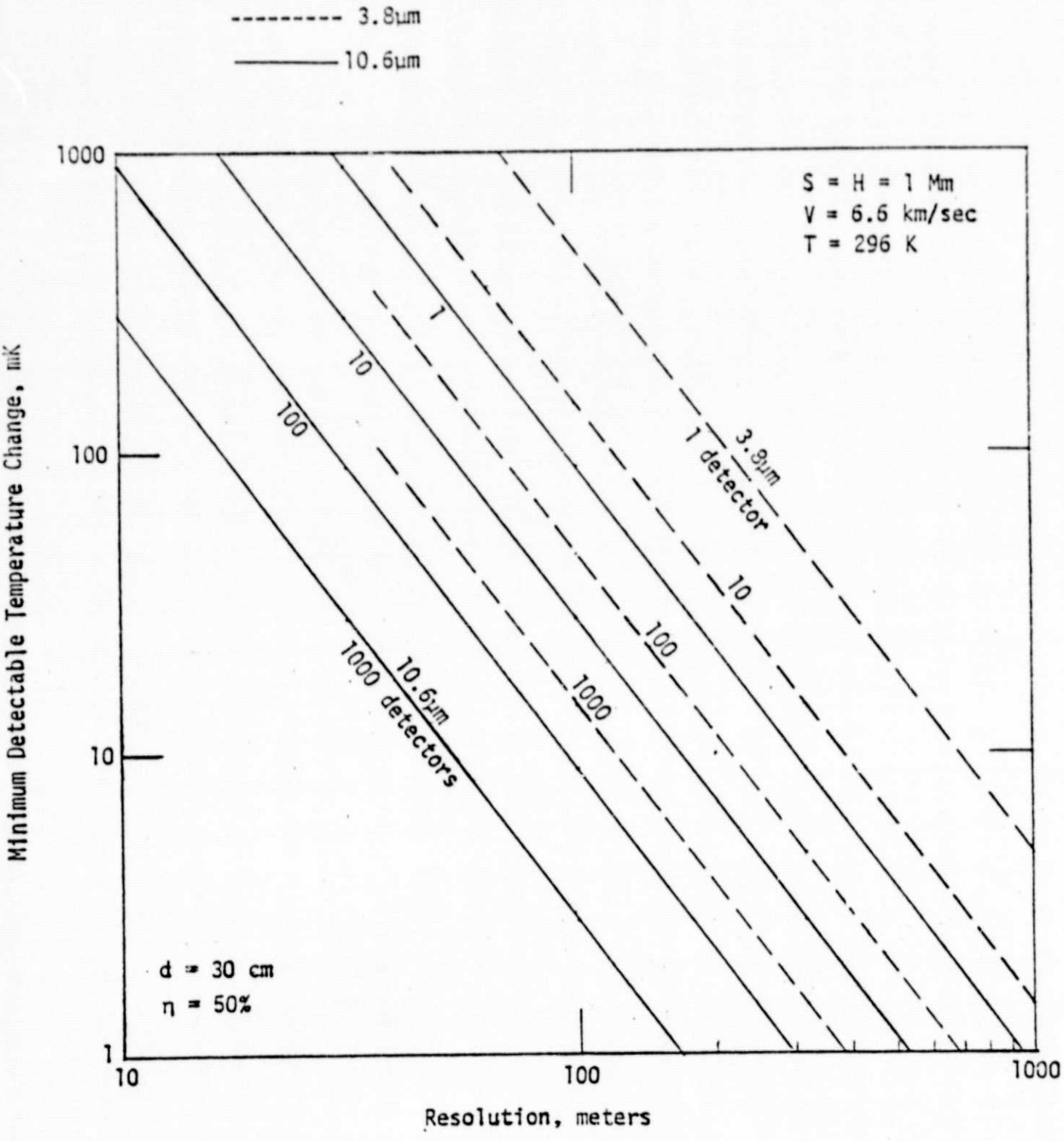

Fig. 7. Performance of Advanced Infrared Imaging Radiometer (shot noise limited) in a Satellite

3.0 MICROWAVE RADIOMETRY

We foresee a limited application of microwave radiometry for pollution sensing from satellites, although there may be some application from aircraft providing they fly beneath the clouds. The reasoning behind this conclusion follows. First, the requirement for angular resolution forces the choice of a short wavelength on the order of λ = 1 cm (F = 30 GHz). But the radiometer is sensitive to clouds at this wavelength, and so its use on a satellite is limited to areas with clear skys. Moreover, at these high frequencies, the radiometer is quite insensitive to sea temperature and conductivity (salinity), as discussed later. The main sensitivity that remains is surface roughness which is of great interest for detection and monitoring of oil slicks.

However, the measurement of roughness puts radiometry into direct competition with radar scatterometry, which measures the same thing. Radar has most of the advantages:

1. penetrates clouds
2. high resolution available by range gating and synthetic aperture
3. no problem with reflected cloud radiance
4. lower frequencies (e.g. L-band) usable if synthetic aperture used for angular resolution
5. cross polarization data

The only advantages for radiometry are:

6. no transmitter power
7. no clutter statistics (random interference effects)

In case of a satellite, Items 1 and 2 appear to be the driving factors. The cloud penetration (1) is very important because 70 to 80% of the ocean is covered by clouds. Also resolution (Item 2) is critical in the satellite

case as we show in Section 3.3. Item 3, problems with reflected cloud radiance is severe because reflectivity is on the order of 50%, depending on frequency and look angle. This may tip the balance in favor of radar even in the aircraft case. The fact that radar requires transmitter power and has problems with clutter statistics (implied by Items 6 and 7) is just something we shall have to work around. These matters are described in the following sections and summarized briefly in Table 3, a sort of 4-dimensional microwave matrix that considers:

- platform: satellite, aircraft
- mode: active (radar), passive (radiometer)
- sky: clear, cloudy
- sensitivity to water condition: roughness, salinity, temperature

3.1 Radiometric Temperature of Seawater

The intensity of radiation recovered in a microwave radiometer is customarily expressed as radiometric temperature T. This would be the same as thermodynamic temperature if the radiometer were pointed at a perfect absorber, but seawater is not, and so a radiometer looking at the sea sees a complicated mix of water and sky radiance reflected from various directions. The results in the case of a clear sky is that the radiometric temperature depends very little on the water temperature except at low frequencies; Stogryn [IEEE Transactions AP-15, p. 278 (Mar 67)] confirms it in a classic paper, for F = 19.4 GHz (λ = 1.5 cm), windspeeds 0 and 7 m/sec and nadir angles 0 and 50^{o}, as shown in Figure 8. Other investigators have found similar results, e.g. a group at Texas A&M, Figures 9 10, and 11. Figure 9 shows considerable dependence on sea temperature at 9.3 GHz (λ = 3.2 cm), but as discussed later, this frequency provides too little angular resolutions. Figures 9, 10, and 11 also show that the radiometer does not respond effectively to salinity, which might be important in some pollution studies.

TABLE 3 MICROWAVE SUMMARY

Mode	Platform	Sensitivity	Sky	
			clear	cloudy
Passive (radiometer)	Satellite	surface roughness	POOR compared to radar which offers far better resolution and the following options: • range gate • synthetic aperture • cross polarization	NO Clouds require $\lambda \gtrsim$ 10cm but angular resolution requires $\lambda \lesssim$ 1 cm
		conductivity (salinity)	NO Sensitive only if $\lambda >$ 3cm, but angular resolution requires $\lambda \lesssim$ 1cm.	
		water temperature	NO Sensitive only if $\lambda \gtrsim$ 10cm, but angular resolution requires $\lambda \lesssim$ 1cm.	

Mode	Platform	Sensitivity	Sky	
			clear	cloudy (fly under?)
Passive (radiometer)	Aircraft	roughness	YES but not superior to radar.	POOR compared to radar since radiometer data complicated by reflected cloud radiance
		conductivity	POOR since measure of conductivity must be disentangled from large effects of surface roughness and clouds	
		temperature	Probably NO since infrared radiometer does the job with far better resolution and less interference from reflected sky and surface roughness.	

Mode	Sensitivity	Sky	
		clear	cloudy
Active (radar)	roughness	YES	
	conductivity	YES if long λ	
	temperature	NO	

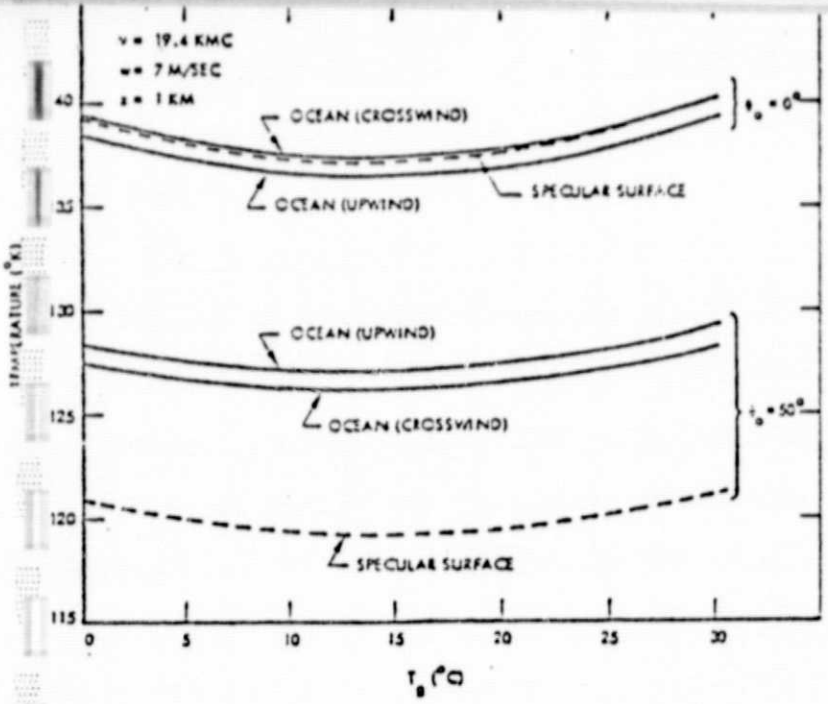

Fig. 8. Temperature of horizontally polarized radiation as a function of water temperature.

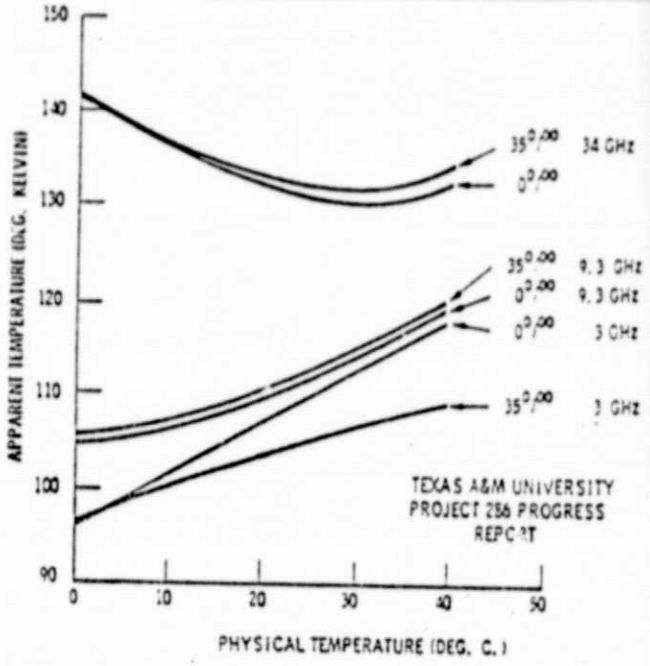

Fig. 9. Theoretically predicted curves. Brightness temperature vs. salinity and temperature.

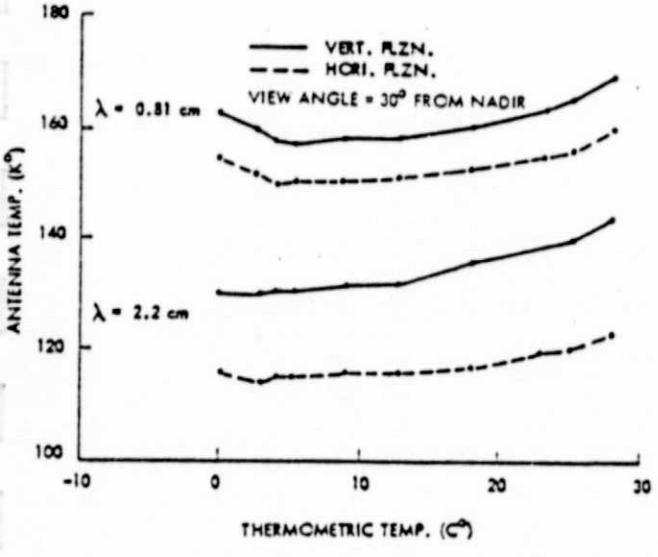

Fig. 10. Antenna brightness temperature of fresh water as a function of thermometric temperature.

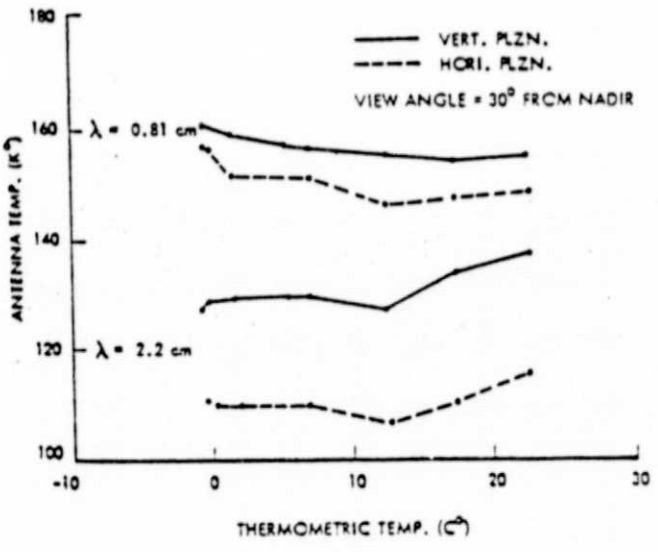

Fig. 11. Antenna brightness temperature of sea water as a function of thermometric temperature.

A microwave radiometer looking at the sea is sensitive to the angle of the water surface, and hence to wind that roughens the surface. This effect appears in curves by Stogryn reproduced here as Figures 12, 13, and 14.

3.2 Clouds

Figures 12 and 14 show that temperature sensitivity on the order of

$$\Delta T = 1 \text{ Kelvin}$$

is needed to sense small changes in surface roughness. This in turn limits the amount of interference that can be tolerated from clouds, ΔT_c. This interference is proportional to the fractional absorption A:

$$\Delta T_{cloud} = AT_c$$

Assuming T_c = 300 Kelvin gives A = .003. Comparing to Figure 15 shows that even a light cloud causes appreciable interference at frequencies 10 GHz or higher. But frequencies this high (see Section 3.3) are required to attain reasonable angular resolution, and so the microwave radiometer, unlike radar, simply will not be very useful in seeing through clouds.

3.3 Instrumental Limitations

The sensitivity of a microwave radiometer to temperature changes is given by

$$\Delta T = \frac{2\ T_n}{\sqrt{B\tau}} \qquad (51)$$

where T_n is the receiver noise temperature, B its bandwidth, and τ the dwell time. The factor of 2 applies strictly to a Dicke radiometer, and varies slightly with other schemes used to stabilize the gain. The dwell time needed for Equation 1 depends on platform velocity V and geometrical factors:

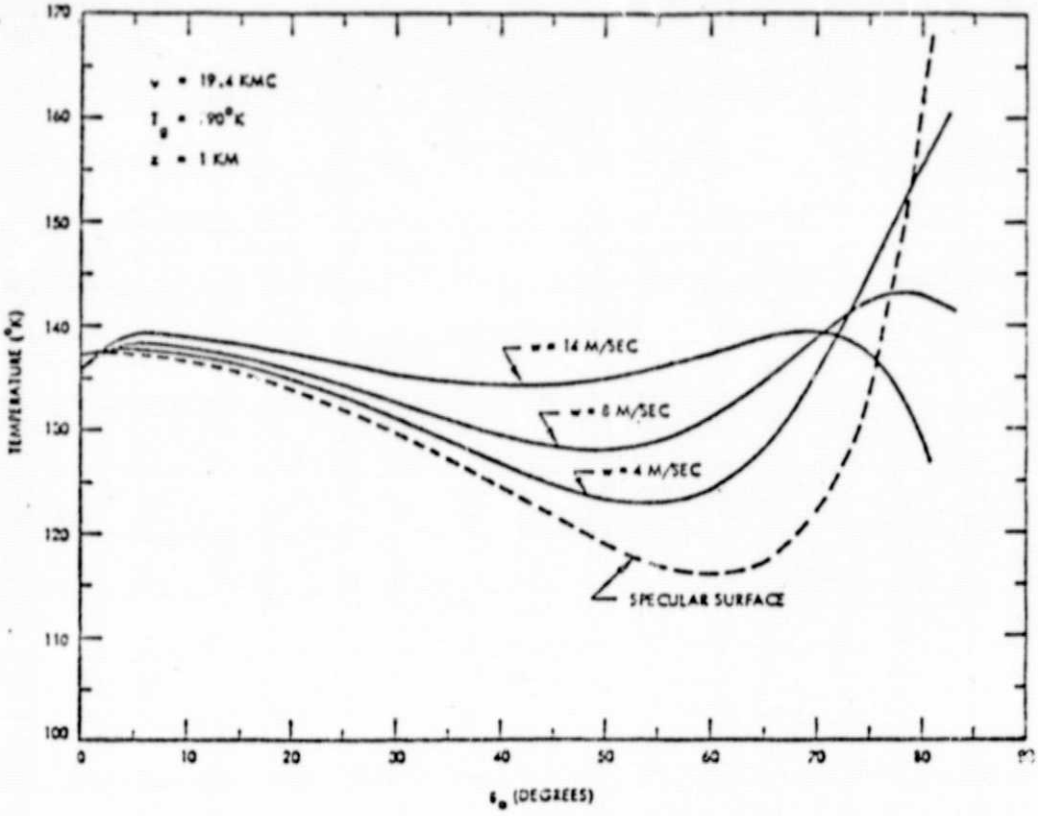

Fig. 12. Temperature of horizontally polarized radiation as a function of angle (upwind case).

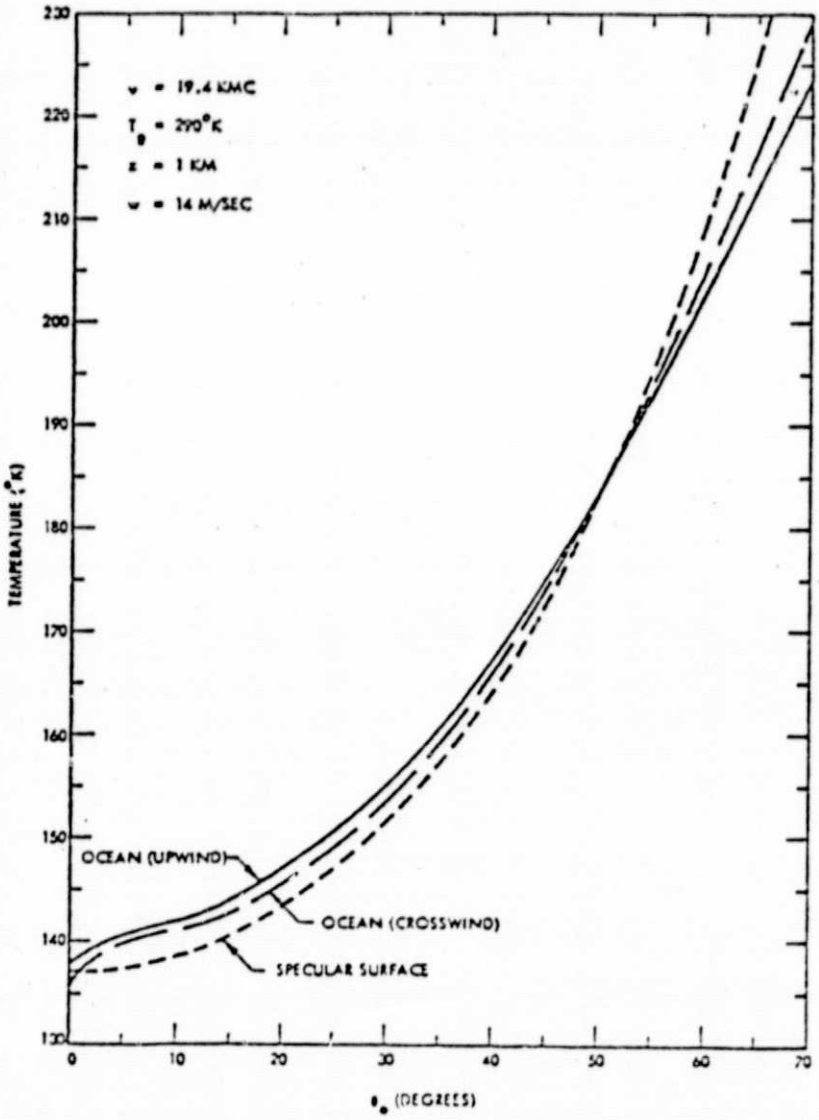

Fig. 13. Temperature of vertically polarized radiation as a function of angle.

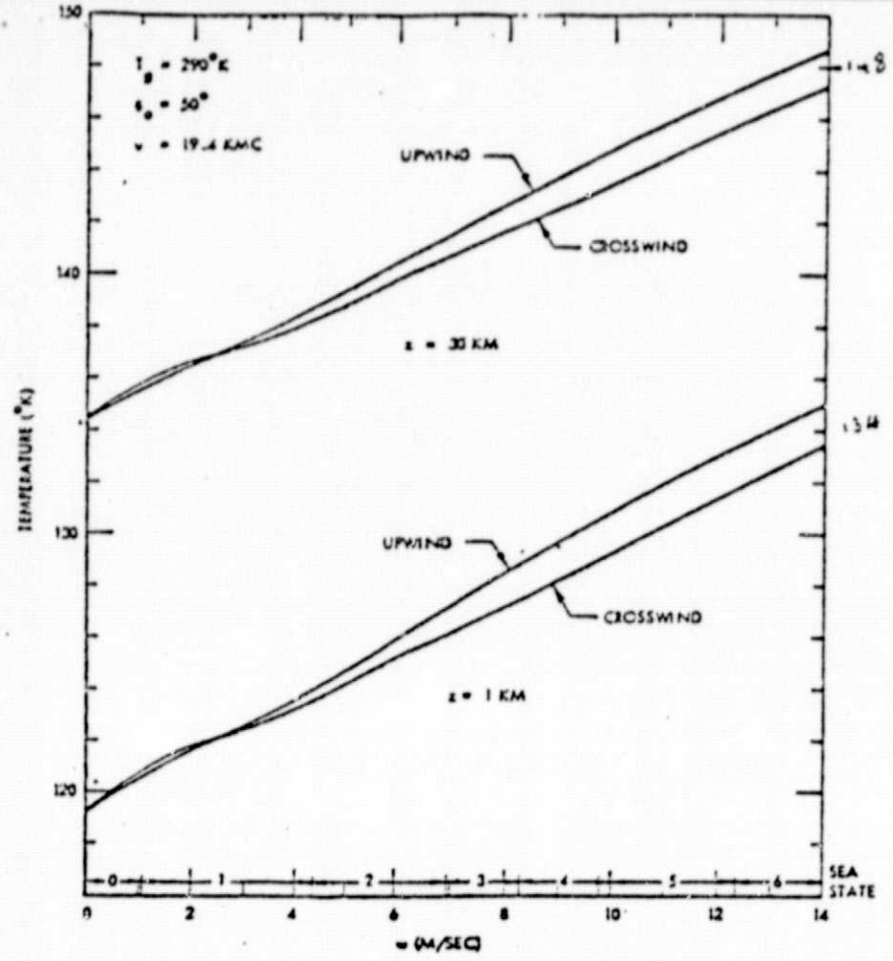

Fig. 14. Temperature of horizontally polarized radiation as a function or wind speed.

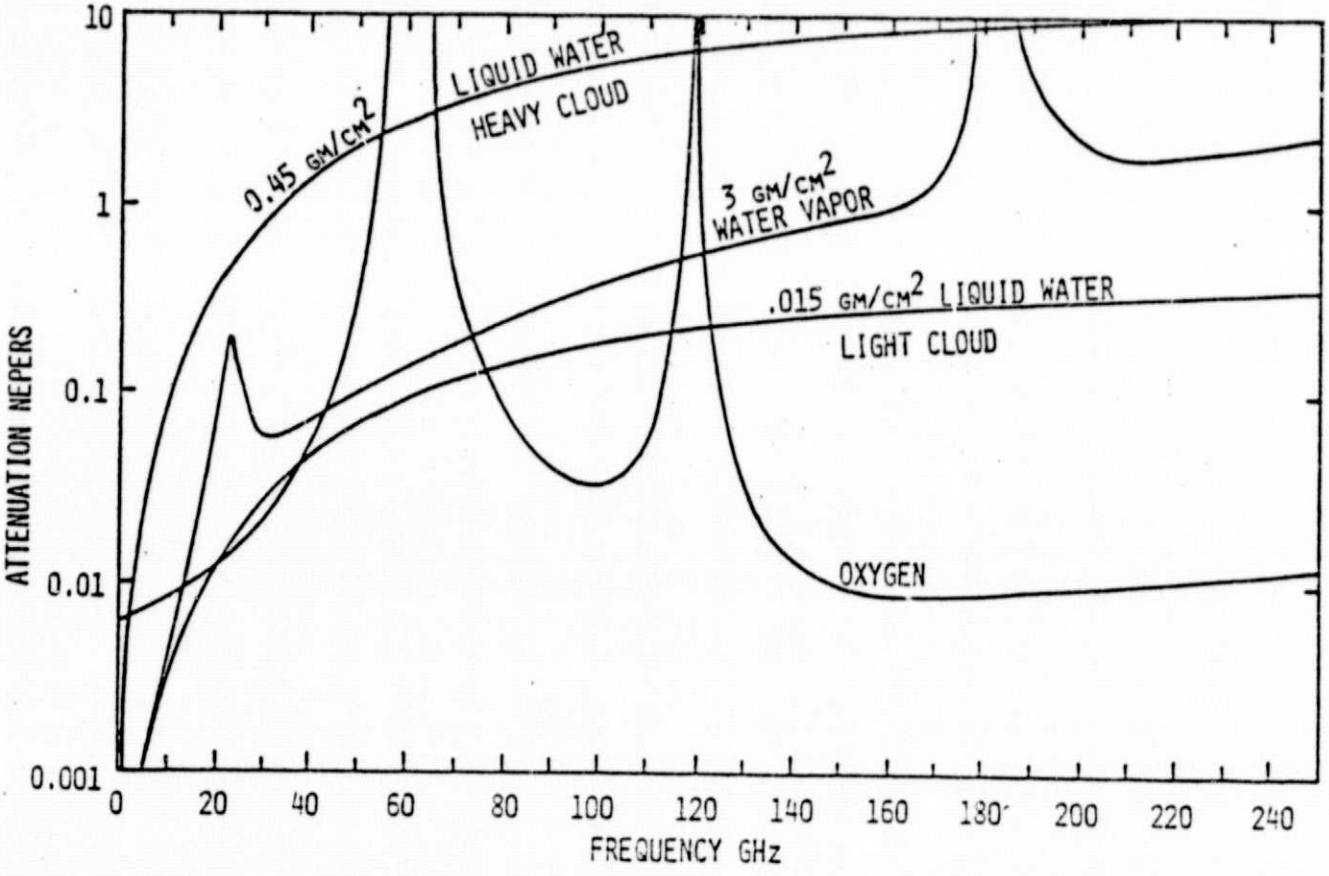

Fig. 15. Zenith microwave opacity components for a standard atmosphere, 3 gm/cm^2 columnar water vapor density and two clouds.

$$\tau = \frac{\text{resolution area}}{\text{area search rate}}$$

$$\tau = \delta^2/SV \qquad (52)$$

where S is the swath width and δ the dimension of a resolution cell (presumed square). At nadir, the resolution is approximately:

$$\delta = \lambda h/d \quad , \qquad (53)$$

where h is altitude and d aperture diameter. This equation expresses a severe bind: λ should be short for good resolution, but long to avoid excessive sensitivity to thin clouds or fog. The best one can do is use large apertures as listed in Table 4 along with assumed λ, h and resulting δ. The value δ = 1 km in the satellite column is adequate for mapping a large oil spill, but too large for many smaller dumps. Other reasonable assumptions are listed in this table along with the results from Equations 51, 52, and 53. These results show that the sensitivity is quite adequate. The real crunch is in resolution and sensitivity to clouds.

TABLE 4 RADIOMETER ASSUMPTIONS AND RESULTS

Assumptions	Satellite	Aircraft
Altitude H	1 Mm	3 km
Swath S = H	1 Mm	3 km
Velocity V	7 km/sec	160 m/s
Wavelength λ	1 cm	3 cm
Frequency F	30 GHz	10 GHz
B = F/10	3 GHz	1 GHz
Aperture diameter d	10m = 1000λ	1 meter = 33λ
Noise temperature T_n	150K	150K
Results		
Resolution δ	1 km	100 m
Dwelling time τ	140μs	20 msec
Sensitivity ΔT	0.46K	.067K

APPENDIX

Curves of Spectral Radiance

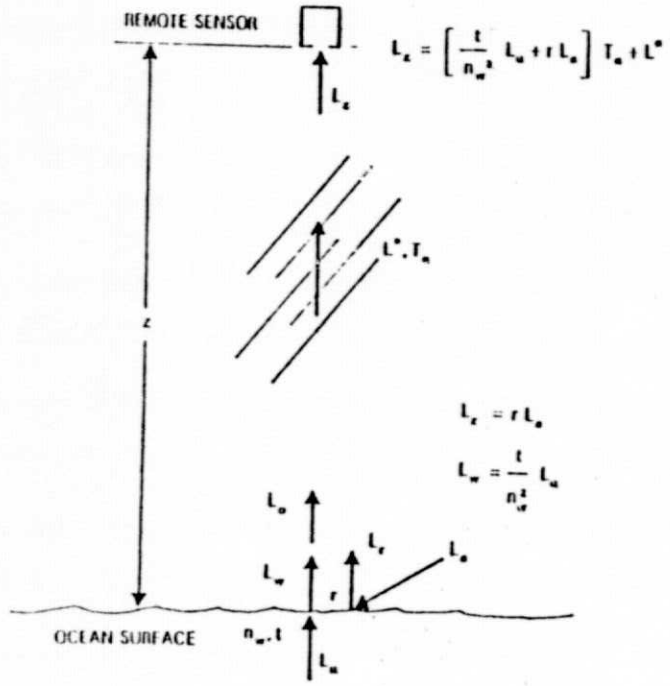

Fig. 11. Component parts of the upwelling radiance signal, L_z.

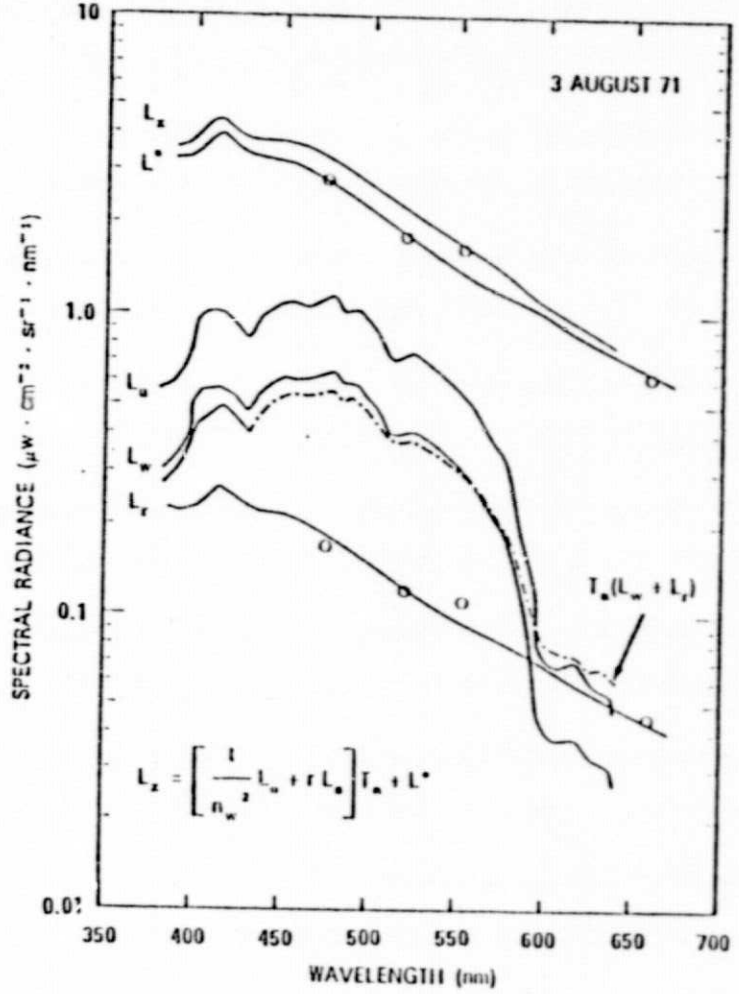

Fig. 12. Computed apparent spectral radiance of the ocean (and its components) as observed above the atmosphere. Blue-green water.

Figures by RW Austin, "Remote Sensing of Spectral Radiance," Chapter 14 in Optical Aspects of Oceanography, edited by NG Jerlov and ES Nielsen, Academic Press, NY 1974 (continued next page)

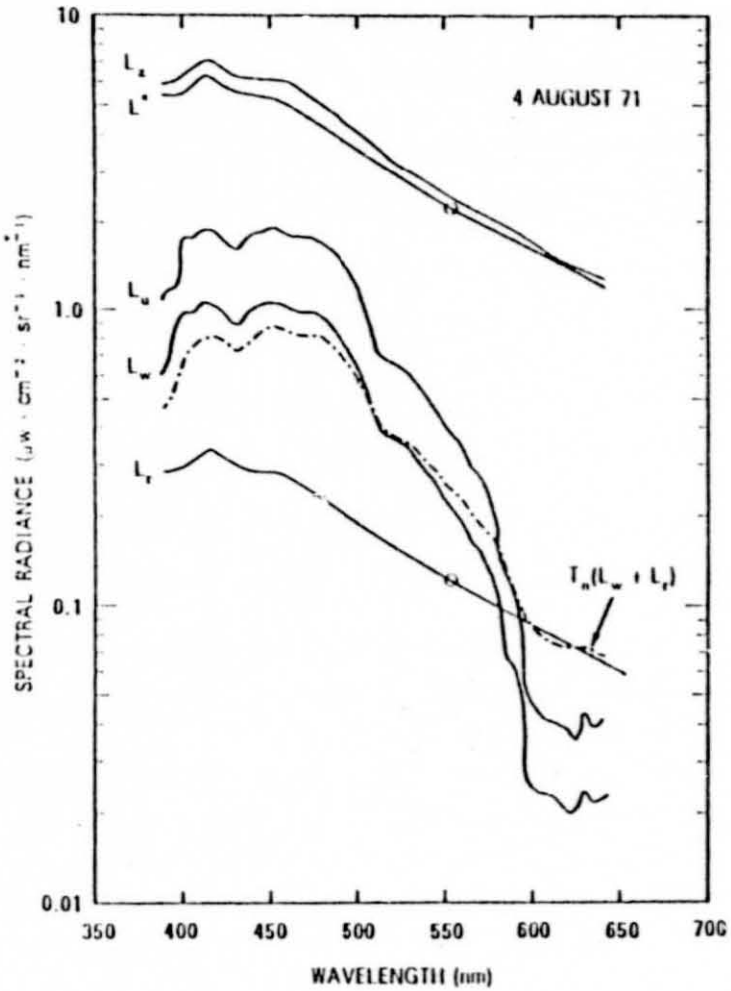

Fig. 13. Computed apparent spectral radiance of the ocean (and its components) as observed above the atmosphere. Blue water.

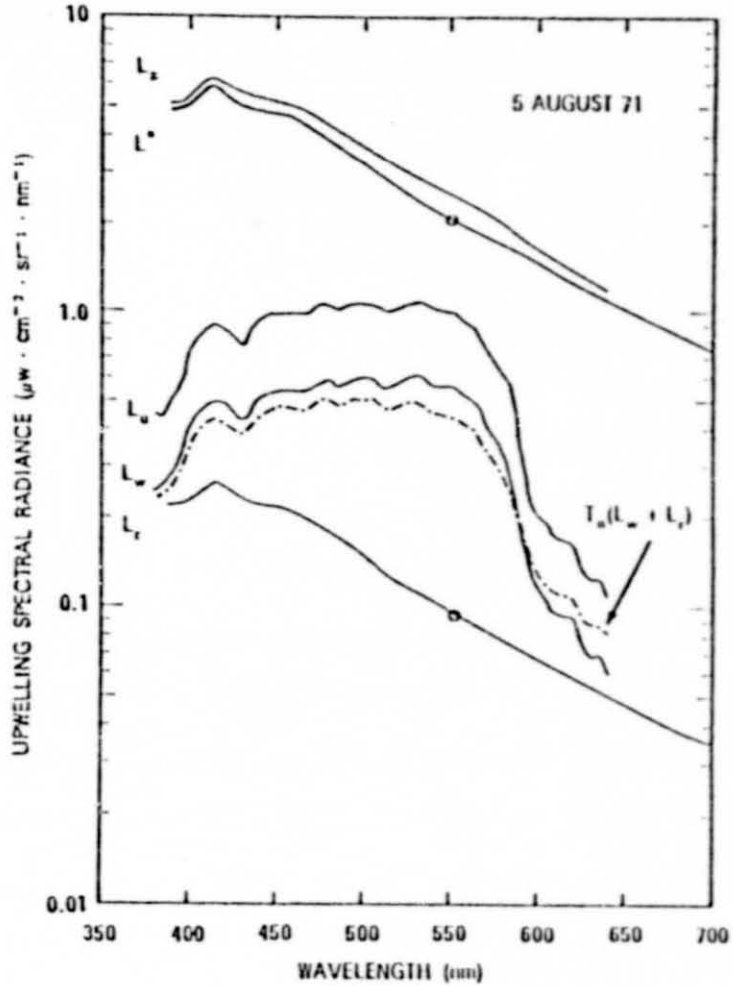

Fig. 14. Computed apparent spectral radiance of the ocean (and its components) as observed above the atmosphere. Green water.

Figures by RW Austin, concluded